DOI:
10.1073/pnas.1919451117

Document Version
Peer reviewed version

Electron-Phonon-Driven Three-Dimensional Metallicity in an Insulating Cuprate

Edoardo Baldini,[1,2] Michael A. Sentef,[3] Swagata Acharya,[4] Thomas Brumme,[3,5] Evgeniia Sheveleva,[6] Ekaterina Pomjakushina,[7] Christian Bernhard,[6] Mark van Schilfgaarde,[4] Fabrizio Carbone,[2] Angel Rubio,[3,8] and Cédric Weber[4]

[1] *Department of Physics, Massachusetts Institute of Technology, Cambridge, Massachusetts, 02139, USA*
[2] *Institute of Physics, Laboratory for Ultrafast Microscopy and Electron Scattering (LUMES), École Polytechnique Fédérale de Lausanne, Lausanne, Switzerland*
[3] *Max Planck Institute for the Structure and Dynamics of Matter, Hamburg, Germany*
[4] *Department of Physics, King's College London, London WC2R 2LS, United Kingdom*
[5] *Wilhelm Ostwald Institut of Physical and Theoretical Chemistry, University of Leipzig, Leipzig, Germany*
[6] *Department of Physics, University of Fribourg, Chemin du Musée 3, CH-1700 Fribourg, Switzerland*
[7] *Solid State Chem. Group, Laboratory for Multiscale Materials Experiments, Paul Scherrer Institute, CH-5232 Villigen PSI, Switzerland*
[8] *Center for Computational Quantum Physics, The Flatiron Institute, 162 Fifth Avenue, New York, NY 10010, USA*

(Dated: September 22, 2019)

The role of the crystal lattice for the electronic properties of cuprates and other high-temperature superconductors remains controversial despite decades of theoretical and experimental efforts. While the paradigm of strong electronic correlations suggests a purely electronic mechanism behind the insulator-to-metal transition, recently the mutual enhancement of the electron-electron and the electron-phonon interaction and its relevance to the formation of the ordered phases has also been emphasized. Here, we combine polarization-resolved ultrafast optical spectroscopy and state-of-the-art dynamical mean-field theory to show the importance of the crystal lattice in the breakdown of the correlated insulating state in an archetypal undoped cuprate. We identify signatures of electron-phonon coupling to specific fully-symmetric optical modes during the build-up of a three-dimensional metallic state that follows charge photodoping. Calculations for coherently displaced crystal structures along the relevant phonon coordinates indicate that the insulating state is remarkably unstable towards metallization despite the seemingly large charge-transfer energy scale. This hitherto unobserved insulator-to-metal transition mediated by fully-symmetric lattice modes can find extensive application in a plethora of correlated solids.

I. INTRODUCTION

The insulator-to-metal transition (IMT) and high-temperature (T_C) superconductivity in cuprates are central topics in condensed matter physics [1, 2]. A crucial roadblock towards a complete understanding of the IMT and the details of the phase diagram in these compounds lies in the strong-correlation problem. Electron-electron correlations have long been thought to be the dominant actor responsible for the IMT, whereas the crystal lattice and the electron-phonon coupling have played a secondary role. As a result, much of our present knowledge about the relevant physics of cuprates has been framed around the two-dimensional Hubbard model.

Recently, this purely electronic scenario has been challenged by a body of work. On the theory side, it is believed that the selective modification of bond lengths and angles can trigger a localization-delocalization transition in the undoped parent compounds [3, 4], or even lead to a concomitant increase of the superconducting T_C [5]. On the experimental side, the interplay between the electron-electron and the electron-phonon interaction has been proposed as an efficient pathway to stabilize superconductivity [6, 7]. The emergent picture is that electronic correlations and electron-phonon coupling cannot be considered as independent entities in the high-T_C problem, but rather as equally fundamental interactions that can mutually enhance each other.

While this intertwined character of different interactions makes cuprates excellent candidates to benchmark new theories in correlated-electron physics, it also renders these solids a puzzling case to understand [8]. First-principles theoretical descriptions that deal with strong correlations are notoriously difficult to handle, and only now powerful methods are becoming available that render the problem tractable on modern computers [5, 9]. At the same time, experimental progress in disentangling intricate interactions relies on the development of novel spectroscopic techniques. In particular, driving complex systems out-of-equilibrium and monitoring their real-time behavior with ultrafast probes [10] has evolved as a promising strategy to uncover the relevance of various microscopic degrees of freedom and the mutual forces between them [11].

The application of ultrafast methods to undoped cuprates has revealed preliminary details on the dynamics underlying the IMT. This was accomplished by photodoping particle-hole pairs in the CuO_2 planes with a short laser pulse while monitoring the change in the optical absorption spectrum with a delayed continuum probe [12, 13]. The extremely fast timescale (40-150 fs) associated with the rise of the low-energy Drude response was found to be imprinted onto the dynamical evolution of the charge-transfer (CT) excitation in the visi-

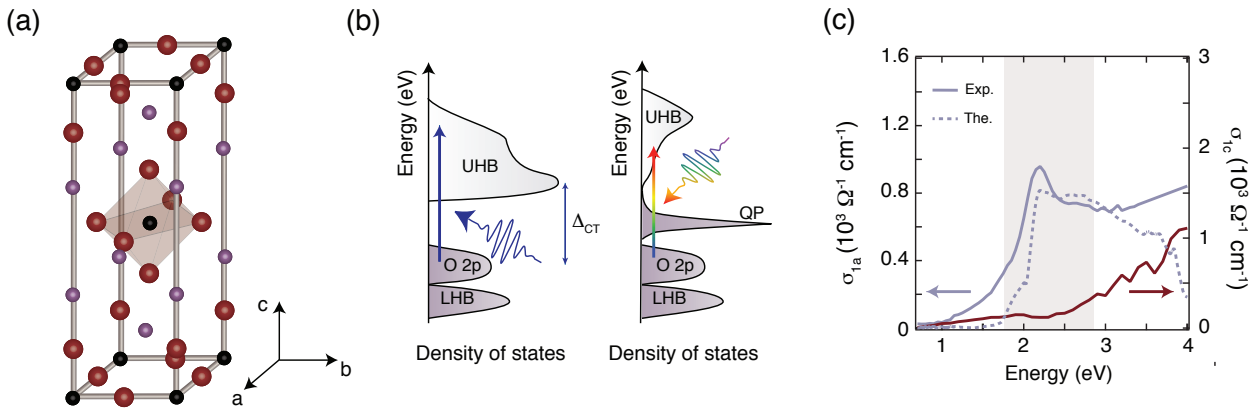

FIG. 1. (a) Crystallographic structure of LCO in its low-temperature orthorhombic unit cell. The Cu atoms are depicted in black, the O atoms in red and the La atoms in violet. (b) Schematics of interacting density of states of undoped insulating (left panel) and photodoped metallic (right panel) LCO with O-2p, Cu-3d lower Hubbard band (LHB) and UHB, and quasiparticle (QP) peak in the metallic case. In the insulating case, the CT gap ($\Delta_{\rm CT}$) is indicated. Blue and multicoloured arrows indicate the 3.10 eV pump and broadband probe pulse photon energies, respectively. (c) Experimental real part of the optical conductivity of LCO at 10 K, measured with the electric field polarized along the a- (violet solid curve) and the c-axis (red solid curve). The shaded area represents the spectral region monitored by the broadband probe pulse in the nonequilibrium experiment. The theory data for the in-plane response calculated with QSGW+DMFT are shown as a violet dashed curve.

ble range. Within 200 fs from its formation, the mobile charges freeze into localized mid-gap states owing to the concomitant action of polar lattice modes and spin fluctuations [14]. Finally, the self-trapped carriers release energy in the form of heat over a picosecond timescale.

Despite being pioneering, these works have left several fundamental questions unanswered. First, the use of cuprate thin films has hindered the study of the charge dynamics along the crystallographic c-axis. Hence, it is unknown whether the transient metallic state has a purely two-dimensional nature or whether it also involves a certain degree of interlayer transport. Furthermore, the high temperature employed in these experiments has masked the observation of possible bosonic collective modes that cooperate with the charge carriers to induce the IMT.

Here we use a powerful combination of ultrafast optical spectroscopy and first-principles calculations to unravel the intricate role of the electron-phonon coupling in the stability of the insulating state of a prototypical cuprate parent compound. By measuring the non-equilibrium response of different elements of the optical conductivity tensor, we reveal that rapid injection of particle-hole pairs in the CuO_2 planes leads to the creation of a three-dimensional (3D) metallic state that has no counterpart among the chemically doped compounds, and is accompanied by a complex motion of the ionic positions along the coordinates of totally symmetric modes. The information gleaned from our experiment about the phonons that strongly couple to the mobile charges is supported by a state-of-the-art theoretical framework that unveils a striking instability of the insulating state against the displacement of the same lattice modes. These findings indicate that the IMT in cuprates cannot be interpreted as a purely electronic effect, calling for the involvement of intertwined degrees of freedom in its dynamics. More generally, these results open an avenue towards the phonon-driven control of the IMT in a wide class of insulators in which correlated electrons are strongly coupled to totally symmetric lattice modes.

II. CRYSTAL STRUCTURE AND EQUILIBRIUM OPTICAL PROPERTIES OF LA_2CUO_4

As a model material system we study La_2CuO_4 (LCO), one of the simplest insulating cuprates exhibiting metallicity upon hole doping. In this solid, the two-dimensional network of corner-sharing CuO_4 units is accompanied by two apical O (aO) atoms below and above each CuO_4 plaquette (Fig. 1(a)). As a result, the main building blocks of LCO are CuO_6 octahedra that are elongated along the c-axis due to the Jahn-Teller distortion. The unit cell of LCO is tetragonal above and orthorhombic below 560 K. A simplified scheme of the electronic density of states is shown in Fig. 1(b) (left panel). The insulating gap ($\Delta_{CT}\sim$2 eV) opens between the filled O-2p band and the unoccupied Cu-3d upper Hubbard band (UHB), thus being of the CT type. In contrast, the occupied Cu-3d lower Hubbard band lies at lower energy.

We first present the optical properties of LCO in equilibrium. Figure 1(c) shows the absorptive part of

the optical conductivity (σ_1), measured via ellipsometry. The in-plane response (σ_{1a}, solid violet curve) is dominated by the excitation across the CT gap at 2.25 eV [15, 16]. This transition is a non-local resonant exciton that extends at least over two CuO_4 units [16, 17]. The strong coupling to the lattice degrees of freedom causes its broadened shape. As such, this optical feature can be modeled as involving the formation of an electron-polaron and a hole-polaron, coupled to each other by a short-range interaction [16, 17]. At higher energy (2.50−3.50 eV), the in-plane spectrum results from charge excitations that couple the O-2p states to both the Cu-3d states in the UHB and the La-5d/4f states. In contrast, the out-of-plane optical conductivity (σ_{1c}, solid red curve) is rather featureless and its monotonic increase with energy is representative of a particle-hole continuum. This spectral dependence reflects the more insulating nature of LCO along the c-axis, which stems from the large interlayer distance between neighboring CuO_2 planes. As a consequence, over an energy scale of 3.50 eV, charge excitations in equilibrium are mainly confined within each CuO_2 plane.

III. PHOTOINDUCED THREE-DIMENSIONAL METALLIC STATE

We now reveal how these optical properties modify upon above-gap photoexcitation. To this aim, we tune the photon energy of an intense ultrashort laser pulse above the in-plane CT gap energy (Fig. 1(b)), photodoping particle-hole pairs into the CuO_2 planes. We explore an excitation regime between 0.023 and 0.075 photons/Cu atom in order to exceed the threshold density needed in LCO for the formation of in-plane metallic conductivity [13]. We then use a continuum probe to map the pump-induced changes of the optical response over the CT energy scale (schematics in Fig. 1(b) and shaded area in Fig. 1(c)). Unlike previous experiments [12, 13, 18], the combination of an (100)-oriented single crystal, an accurate polarization-resolved pump-probe analysis, and low temperature, allow us to identify hitherto undetected details of the light-induced IMT.

Figures 2(a,b) show the spectro-temporal evolution of the a- ($\Delta\sigma_{1a}$) and c-axis ($\Delta\sigma_{1c}$) differential optical conductivity in response to in-plane photoexcitation. Transient spectra at representative time delays are displayed in Fig. 2(c,d). These data are obtained from the measured transient reflectivity through a differential Lorentz analysis [19, 20], which avoids the systematic errors of Kramers-Kronig transformations on a finite energy range.

Injecting particle-hole pairs in the CuO_2 planes produces a sudden reduction in $\Delta\sigma_{1a}$ close to the CT excitation and to its delayed increase to positive values in the 1.80-2.00 eV range (Fig. 2(a,c)). As explained in previous studies [12, 13], this behavior stems from the pump-induced redistribution of spectral weight from high to low energy due to several processes, among which the ultrafast emergence of in-plane metallicity, charge localization in mid-gap states and lattice heating. In particular, the latter causes the first derivative-like shape that gradually arises after several hundreds of femtoseconds and becomes dominant on the picosecond timescale (compare the curve at 1.50 ps in Fig. 2(b) and $\Delta\sigma_{1a}$ of Fig. S2(c) produced by the lattice temperature increase).

The same photodoping process also impacts on $\Delta\sigma_{1c}$ (Fig. 2(b,d)), which is unveiled here for the first time. At 0.10 ps, a crossover between a reduced and an increased $\Delta\sigma_{1c}$ emerges around 2.00 eV. Subsequently, the intensity weakly drops over the whole spectrum and relaxes into a negative plateau that persists for picoseconds while the system thermalizes to equilibrium. The response is featureless and one order of magnitude smaller than its in-plane counterpart. Here we show that this suppressed background is key to unraveling invaluable information of the intricate dynamics of LCO.

First, we compare the temporal evolution of $\Delta\sigma_1$ along the two crystallographic axes and focus on the dynamics close to zero time delay. Figure 2(e) displays a representative trace of $\Delta\sigma_{1a}$ obtained through integration around the CT feature. The intensity drops within ∼0.17 ps, a timescale that is significantly longer than our resolution (∼0.05 ps). The subsequent relaxation spans tens of picoseconds [12, 13]. A close inspection around zero time delay (inset of Fig. 2(e)) reveals a resolution-limited signal that emerges only partially before being buried under the pronounced intensity drop. Figure 2(f) shows the out-of-plane response (integrated over the low-energy region of Fig. 2(d)), which shares important similarities with the in-plane signal: The intensity suppression is also complete within ∼0.17 ps and comprises a resolution-limited feature that perfectly mirrors the one along the a-axis. This signal cannot originate from a leakage of the other probe polarization channel, as the shape of the $\Delta\sigma_{1c}$ spectrum has no fingerprint of the in-plane CT exciton. Furthermore, since the resolution-limited temporal response is only observed in LCO and over a broad spectral range away from the pump photon energy, it cannot be a pump-induced artifact (see §S4). Conversely, the combination of high time resolution and a continuum probe allows us to ascribe this feature to the signature imprinted onto the CT energy scale by a light-induced metallic state [12, 13].

This conclusion naturally emerges through direct inspection of our spectro-temporal response. In the time domain, the rise of $\Delta\sigma_{1a}$ is in excellent agreement with the evolution of the Drude conductivity found by Okamoto et al. [13] and $\Delta\sigma_{1c}$ closely mimics $\Delta\sigma_{1a}$. Quantitative information is gained through a systematic analysis of the dynamics along both crystallographic axes. This is obtained through a global fit of the temporal traces over the whole range. An accurate fit is accomplished only through a model based on that proposed by Okamoto et al. [13]: A Gaussian function representing the metallic state captures the fast-varying signal during the rise of the response, whereas a subse-

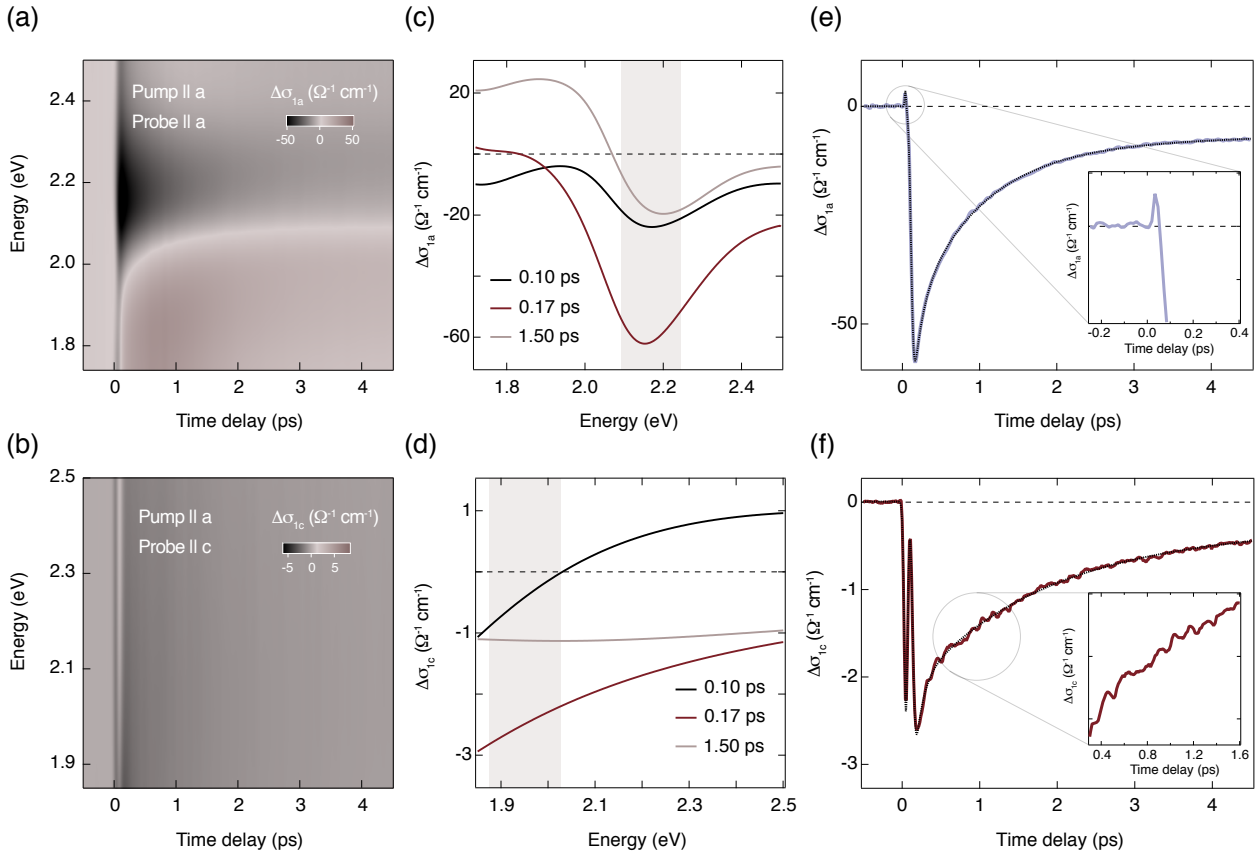

FIG. 2. (a,b) Color-coded maps of the differential optical conductivity $\Delta\sigma_1$ at 10 K with in-plane pump polarization and (a) in-plane, (b) out-of-plane probe polarization, as a function of probe energy and pump-probe delay time. The pump photon energy is 3.10 eV and the excitation photon density is $x_{ph} \sim 0.06$ photons/Cu. For in-plane probe polarization (a), we observe a significantly reduced $\Delta\sigma_1$ above the CT edge at 1.80 eV, due to the spectral weight redistribution to lower energies. For out-of-plane probe polarization, the depletion in $\Delta\sigma_1$ is considerably weaker and rather featureless. Oscillatory behavior is visible in the color-coded map hinting at coherently excited phonon modes. (c,d) Snapshots of the same data as in (a,b) at three different pump-probe delay times during the rise (0.10 ps and 0.17 ps) and the relaxation (1.50 ps) of the response. (e,f) Temporal traces of $\Delta\sigma_1$ along the a- and c-axis. Each temporal trace results from the integration over the energy window indicated by the shaded areas in (c,d). The in-plane trace (e) shows a dramatic suppression and slow recovery without clearly visible coherent oscillations. A small peak emerges in the rise of the response, due to the light-induced metallic state (inset). The out-of-plane trace (f) shows a clear signal that mimics the fast in-plane response, but relaxes with a tail exhibiting pronounced coherent oscillations (highlighted in the inset).

quent multi-exponential relaxation comprises contributions from charge localization in mid-gap states and lattice heating effects. Details are given in §S6; here we only present fits to the traces of Fig. 2(e,f), which are overlapped as dashed black lines.

Besides leaving a characteristic signature in the time domain, the metallic state also impacts the ultrafast spectral response of LCO. A similar behavior appears in both the absorptive and dispersive components of $\Delta\sigma_a$ and $\Delta\sigma_c$ (Figs. S10-S11), but with a time lag between the two directions. This suggests that the metallic state has a 3D character but still remains anisotropic in its temporal evolution. We stress that this 3D metallic state in photodoped LCO is significantly different from the case of chemically-doped LCO [21]. In the latter, 3D metallicity is suppressed up to doping levels as high as $p = 0.12$ (i.e., well above our photodoping density), and only in overdoped samples a well-defined Drude response emerges [22]. In contrast, our findings break the scenario of an ultrafast IMT solely governed by two-dimensional quasiparticles in the CuO_2 planes.

IV. COLLECTIVE MODES DYNAMICS

As a next step, we search for possible collective modes that strongly couple to the mobile carriers and clarify their involvement in the IMT. In this respect, we note that the lack of a significant background in $\Delta\sigma_{1c}$ uncovers a pronounced oscillatory pattern that emerges from the

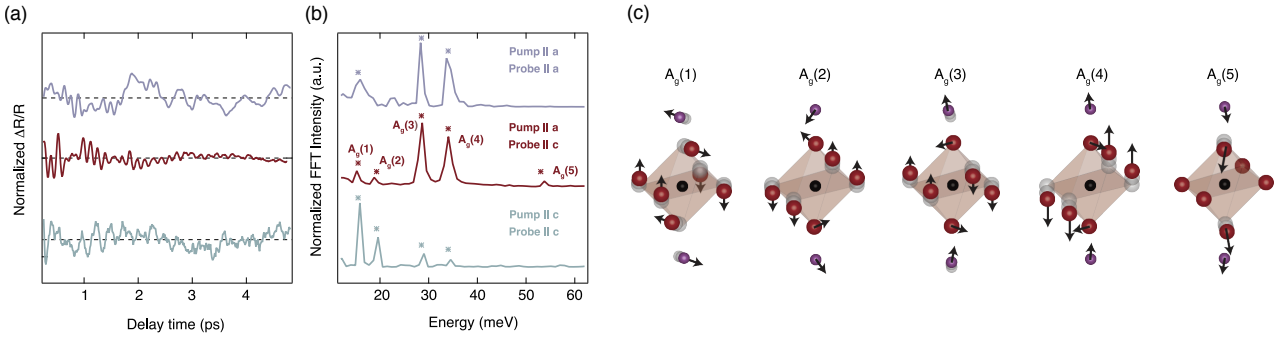

FIG. 3. (a) Residual reflectivity change (normalized to largest amplitudes) after subtraction of recovering background, exhibiting coherent oscillations due to collective bosonic modes. (b) Fast Fourier transform of data in (a). Data in panels (a) and (b) are for different pump and probe polarizations as indicated in (b). The traces have been selected in the probe spectral region that maximizes the oscillatory response (2.00-2.20 eV for the violet curve, 1.80-2.20 eV for the red and the green curves). Different polarizations show the presence of a set of totally symmetric (A_g) phonon modes of the orthorhombic crystal structure. (c) Calculated eigenvectors of the five A_g modes of LCO at $q = 0$. Black atoms refer to Cu, red atoms to O and violet atoms to La. The phonon spectrum has been computed using density-functional theory.

rise of the response and persists during its decay (inset of Fig. 2(f)). This coherent beating is due to collective modes displaced through the delocalized carrier density [23]. Similar oscillations also appear in the a-axis polarization channel (Fig. 2(e)), but the contrast to resolve them is lower owing to the huge relaxation background.

We assign the modes coupled to the in-plane charge density by applying a Fourier filter to the original background-free transient reflectivity data to maintain high accuracy. The results, shown in Fig. 3(a,b), reveal that five bosonic excitations (labelled as $A_g(1-5)$) participate in the non-equilibrium response. Their energies match those of the five A_g phonons reported in orthorhombic LCO by spontaneous Raman scattering [24]. We characterize their ionic displacements by calculating the phonon spectrum of LCO via density-functional theory (see Methods section). Figure 3(c) shows these displacements in the first half cycle of the five A_g phonons. Modes $A_g(1)$ and $A_g(2)$ involve staggered rotations of CuO_6 octahedra. In particular, $A_g(1)$ is the soft phonon of the orthorhombic-to-tetragonal transition. $A_g(3)$ and $A_g(4)$ present large c-axis displacements of the La atom, which in turn modify the La-aO distance. The only difference between them lies in the displacement of the aO: While its out-of-plane motion is the same, its in-plane motion occurs in opposite direction. Lastly, $A_g(5)$ is the breathing mode of the aO. The Fourier transform indicates that all phonons modulate the out-of-plane response (Fig. 3(b), red line), whereas only $A_g(1)$, $A_g(3)$ and $A_g(4)$ are unambiguously resolved in the in-plane signal (Fig. 3(b), violet line). Furthermore, since $A_g(1)$, $A_g(2)$ and $A_g(4)$ are characteristic phonons of orthorhombic LCO [24], their presence confirms the non-thermal nature of the light-induced IMT, as the trajectory followed by the lattice after photodoping does not evolve through the structural phase transition. Finally, no modes with symmetry other than A_g appear in our data. While this result is natural when the probe is c-axis-polarized because of symmetry arguments, more noteworthy is the in-plane probe polarization case. According to Raman selection rules, modes of B_{1g} symmetry should also emerge in this polarization configuration [25]. Their absence can be attributed either to the short lifetime of the B_{1g} component of the real charge-density fluctuation driving the coherent lattice response [23], or to a weak Raman cross-section in the probed spectrum.

To establish which A_g modes preferentially couple to the in-plane photodoped carriers, we also excite LCO with a light field polarized along the c-axis. Despite keeping the carrier excitation density constant, this pump scheme causes a smaller drop in the transient signal amplitude and a weaker modulation depth due to the coherent lattice modes (Fig. S7). Fourier transforming the background-free data (Fig. 3(a,b), green curves) establishes that only $A_g(1)$ and $A_g(2)$ are efficiently triggered by the out-of-plane electronic density, whereas $A_g(3)$ and $A_g(4)$ are strongly suppressed compared to the in-plane photoexcitation scheme. This suggests that periodic structural elongations and compressions of the CuO_6 octahedra along the c-axis through the La atom are favorably triggered by photodoping charges within the CuO_2 planes. This aspect can be explained by noting that excitation across the CT gap promotes electrons in the UHB and holes in the O-2p band, thus locally removing the Jahn-Teller distortion on the CuO_6 octahedra. In the past, this picture has been explored theoretically for chemical (hole) doping, showing how the aO approaches the Cu^{2+} ions to gain attractive electrostatic energy. Consistent with this idea, the dominant mode in our experiment involves coherent displacements of the aO and the La atoms along the c-axis, that is, an oscillating motion that likely follows the destabilization of the

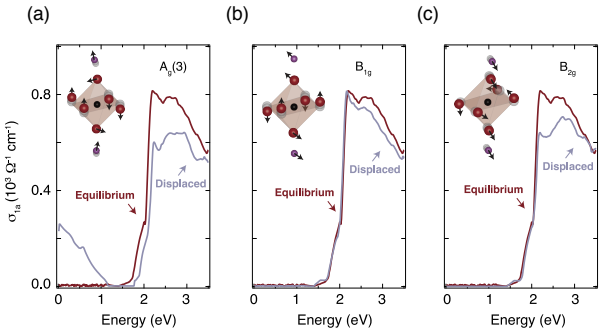

FIG. 4. (a-c) Theory data from QSGW+DMFT simulations of in-plane optical conductivity for the LCO unit cell displaced by 0.04 $\AA$ along different phonon coordinates as indicated. For displacement along totally symmetric A_g modes, with one representative example shown in (a), metallization occurs with spectral weight appearing at low energy below $\sim$ 1.00 eV. In contrast, for displacements along B_g modes (b,c) there is no metallization and hardly any impact on the low-energy spectral weight inside the CT gap.

Jahn-Teller distortion.

V. ROLE OF THE ELECTRON-PHONON COUPLING IN THE INSULATOR-TO-METAL TRANSITION

Our results indicate that the ultrafast 3D metallization of LCO is accompanied by a complex structural motion that is strongly coupled to the delocalized carriers. It is therefore crucial to clarify whether the ionic displacements along the relevant lattice mode coordinates can also dramatically change the electronic properties of LCO. To this end, we perform advanced calculations using dynamical mean-field theory on top of a quasiparticle self-consistent GW approach (QSGW+DMFT, see Methods). This recently-developed method offers a non-perturbative treatment of the local spin fluctuations that are key for the electronic properties of undoped cuprates. We benchmark this technique on the in-plane equilibrium optical properties of LCO. Figure 1(c) shows the calculated σ_{1a} for an undisplaced unit cell (dashed violet line). There is remarkable quantitative agreement with the experimental data, which strongly validates our theory and marks an important step forward in the computational treatment of correlated insulators. Previous attempts obtained only a limited description of the optical absorption onset [26], while our approach accurately captures the d-p correlations that are pivotal for the Madelung energy [27].

Using this method, we address the influence of distinct long-wavelength lattice modes on the electronic structure and optical properties of LCO. We compute the single-particle spectral properties and optical conductivity within the frozen-phonon approximation, *i.e.* by statically displacing the ions in the unit cell along the coordinates of relevant Raman-active modes. Figure 4(a-c) shows representative results, whereas Figs. S13-S14 provide the full analysis. Surprisingly, we observe that displacements along each of the A_g modes tend to induce net metallization. The system evolves into a bad metal with an incoherent quasiparticle peak in the single-particle spectral function and a broad Drude response in σ_{1a}. In contrast, modes with symmetries other than A_g cause no metallic instability. These results have two important implications: i) The spectral region covered by our experiment is sensitive to the displacements of modes with any symmetry, ruling out the possibility of a weak Raman cross-section behind the lack of B_{1g} modes in our experiment; ii) Only displacements with a totally symmetric representation induce the IMT.

Let us discuss the possible contributions that can explain the observed metallicity in the A_g-displaced structures: effective doping, change of screening, and modification of orbital overlaps. Regarding the doping into Cu-3d states, displacements along the coordinates of all Raman-active modes (except B_{3g}) lead to an increase in the hole density in the d states relative to the undisplaced case (Table S2 of the Supplemental Materials). For the B_g modes this effective doping yields $\sim$0.4% holes for B_{1g}, $\sim$0.3% holes for B_{2g} and $\sim$1.5% electrons for B_{3g}, respectively. For the A_g modes (except $A_g(1)$), the hole doping reaches significantly larger values of more than $\sim$3%. It appears that all the Raman-active modes that cause significant effective doping in Cu-3d states transfer spectral weight to lower energies, leading to weak metallization. Enhanced screening in the displaced structures could also lead to the breakdown of the insulating states via modified effective Hubbard U and CT energies. However, our estimates of the CT energy for the displaced structures show very small variation compared to that of undisplaced LCO (Table S1 of the Supplemental Materials). While these changes are typically larger for modes that lead to metallization, the rather small modification of the CT energy alone is unlikely to cause the loss of the insulating state. Finally, by the principle of exclusion, the orbital overlaps and thus the hopping integrals between Cu-3d and O-2p orbitals remain as the main explanation for the observed metallization, due to their high sensitivity to certain lattice displacements. While we do not explicitly compute values for renormalized hoppings here, the momentum-resolved spectral functions for the displaced structures (Fig. S13) strongly suggest that modified hoppings are indeed the most important ingredient for the observed metallization.

VI. CONCLUSIONS

The fundamental and technological implications of our results are noteworthy. On the theory side, we have reported a hitherto undetected type of IMT, which applies

to pure Mott/CT insulators (i.e. devoid of coexisting charge-orbital orders [28–30] and not lying in proximity to a structural transformation [31–33]) and can therefore be extended to a wide class of correlated solids such as iridates, manganites, or NiO. Moreover, in the specific case of cuprates, our data enrich the debate around the role of electron-phonon interactions [6, 7, 34–41]. An old puzzle in the field is the absence of quasiparticles in the filling-driven Mott transition [42, 43], related to the chemical-potential jump between electron- and hole-doped cuprates [44]. Our results add new insights to this picture. First, the combination of our equilibrium optical data and calculations reinforces the idea that polar lattice modes cooperate with the electronic correlations to freeze quasiparticles and stabilize the insulating state of LCO [12–14, 18, 45]: This is evidenced by the polaronic spectral weight extending in Fig. 1(c) down to 1.00 eV, at odds with the 1.80 eV gap retrieved by simulations that neglect coupling to (virtual) phonons. On top of this, our study reveals that (real) Raman-active lattice displacements can induce quasiparticle delocalization in the driven state. Taken together, these results constitute additional proof for the role of the crystal lattice both for quasiparticle dressing and stability towards metallization, and indicate that the strong-correlation problem is incomplete without phonons.

On the applied side, the important upshot from our findings is that selective excitation of Raman-active modes bears huge potential for the control of the IMT in correlated insulators. In recent years, the notion of nonlinear phononics has opened an avenue towards the lattice-mediated control of electronic properties in a wide variety of doped correlated materials [46, 47]. The underlying mechanism involves the resonant excitation of large-amplitude polar modes, whose oscillation displaces the crystal along the coordinates of coupled Raman-active modes. Extending these studies to the insulating parent compounds by employing narrow-band THz fields and sum-frequency ionic Raman scattering [48, 49] will realize the mode-selective control of the IMT, paving the way to the use of these solids in fast room-temperature devices. Finally, our joint experimental-theoretical effort points to rational-design strategies for novel quantum materials that exhibit a subtle interplay of electron-electron and electron-phonon interactions.

ACKNOWLEDGMENTS

We thank Anthony J. Leggett, Antoine Georges, and Ferdi Aryasetiawan for insightful discussions and Zhi-Xun Shen for the critical reading of our paper. T.B. and A.R. were supported by the European Research Council (ERC-2015-AdG694097) and European Union H2020 program under GA no.676580 (NOMAD). M.A.S. acknowledges financial support by the DFG through the Emmy Noether programme (SE 2558/2-1). This work was supported by EPSRC (EP/R02992X/1, EP/N02396X/1, EP/M011631/1), and the Simons Many-Electron Collaboration. E.S. and C.B. acknowledge funding from the SNSF by Grant No. 200020-172611. For computational resources, S.A., M.v.S. and C.W. we were supported by the ARCHER UK National Supercomputing Service and the UK Materials and Molecular Modelling Hub for computational resources (EPSRC Grant No. EP/ P020194/1); T.B. was supported by the MPCDF Garching.

* ebaldini@mit.edu
** michael.sentef@mpsd.mpg.de
*** cedric.weber@kcl.ac.uk

VII. BIBLIOGRAPHY

[1] P. A. Lee, N. Nagaosa, and X.-G. Wen, *Doping a Mott insulator: Physics of high-temperature superconductivity*, Rev. Mod. Phys. **78**, 17 (2006).
[2] B. Keimer, S. A. Kivelson, M. R. Norman, S. Uchida, and J. Zaanen, *From quantum matter to high-temperature superconductivity in copper oxides*, Nature **518**, 179 (2015).
[3] C. Weber, C. Yee, K. Haule, and G. Kotliar, *Scaling of the transition temperature of hole-doped cuprate superconductors with the charge-transfer energy*, EPL (Europhysics Letters) **100**, 37001 (2012).
[4] P. Cai, W. Ruan, Y. Peng, C. Ye, X. Li, Z. Hao, X. Zhou, D.-H. Lee, and Y. Wang, *Visualizing the evolution from the Mott insulator to a charge-ordered insulator in lightly doped cuprates*, Nat. Phys. **12**, 1047 (2016).
[5] S. Acharya, C. Weber, E. Plekhanov, D. Pashov, A. Taraphder, and M. Van Schilfgaarde, *Metal-insulator transition in copper oxides induced by apex displacements*, Phys. Rev. X **8**, 021038 (2018).
[6] O. Gunnarsson and O. Rösch, *Interplay between electron–phonon and Coulomb interactions in cuprates*, J. Phys.: Condens. Matter **20**, 043201 (2008).
[7] Y. He, M. Hashimoto, D. Song, S.-D. Chen, J. He, I. Vishik, B. Moritz, D.-H. Lee, N. Nagaosa, J. Zaanen, *et al.*, *Rapid change of superconductivity and electron-phonon coupling through critical doping in Bi-2212*, Science **362**, 62 (2018).
[8] E. Fradkin, S. A. Kivelson, and J. M. Tranquada, *Colloquium: Theory of intertwined orders in high temperature superconductors*, Rev. Mod. Phys. **87**, 457 (2015).
[9] D. Golež, L. Boehnke, M. Eckstein, and P. Werner, *Dynamics of photodoped charge transfer insulators*, Phys. Rev. B **100**, 041111 (2019).
[10] C. Giannetti, M. Capone, D. Fausti, M. Fabrizio, F. Parmigiani, and D. Mihailovic, *Ultrafast optical spectroscopy of strongly correlated materials and high-temperature superconductors: A non-equilibrium approach*, Adv. Phys. **65**, 58 (2016).
[11] M. Sentef, A. F. Kemper, B. Moritz, J. K. Freericks, Z.-X. Shen, and T. P. Devereaux, *Examining electron-boson coupling using time-resolved spectroscopy*, Phys. Rev. X **3**, 041033 (2013).
[12] H. Okamoto, T. Miyagoe, K. Kobayashi, H. Uemura, H. Nishioka, H. Matsuzaki, A. Sawa, and Y. Tokura, *Ultrafast charge dynamics in photoexcited Nd_2CuO_4 and*

La_2CuO_4 cuprate compounds investigated by femtosecond absorption spectroscopy, Phys. Rev. B **82**, 060513 (2010).

[13] H. Okamoto, T. Miyagoe, K. Kobayashi, H. Uemura, H. Nishioka, H. Matsuzaki, A. Sawa, and Y. Tokura, *Photoinduced transition from Mott insulator to metal in the undoped cuprates Nd_2CuO_4 and La_2CuO_4*, Phys. Rev. B **83**, 125102 (2011).

[14] A. Mishchenko, N. Nagaosa, Z.-X. Shen, G. De Filippis, V. Cataudella, T. Devereaux, C. Bernhard, K. W. Kim, and J. Zaanen, *Charge dynamics of doped holes in high T_c cuprate superconductors: A clue from optical conductivity*, Phys. Rev. Lett. **100**, 166401 (2008).

[15] S. Uchida, T. Ido, H. Takagi, T. Arima, Y. Tokura, and S. Tajima, *Optical spectra of $La_{2-x}Sr_xCuO_4$: Effect of carrier doping on the electronic structure of the CuO_2 plane*, Phys. Rev. B **43**, 7942 (1991).

[16] J. P. Falck, A. Levy, M. A. Kastner, and R. J. Birgeneau, *Charge-transfer spectrum and its temperature dependence in La_2CuO_4*, Phys. Rev. Lett. **69**, 1109 (1992).

[17] D. S. Ellis, J. P. Hill, S. Wakimoto, R. J. Birgeneau, D. Casa, T. Gog, and Y.-J. Kim, *Charge-transfer exciton in La_2CuO_4 probed with resonant inelastic x-Ray scattering*, Phys. Rev. B **77**, 060501 (2008).

[18] F. Novelli, G. De Filippis, V. Cataudella, M. Esposito, I. Vergara, F. Cilento, E. Sindici, A. Amaricci, C. Giannetti, D. Prabhakaran, *et al.*, *Witnessing the formation and relaxation of dressed quasi-particles in a strongly correlated electron system*, Nat. Commun. **5**, 5112 (2014).

[19] B. Mansart, M. J. Cottet, T. J. Penfold, S. B. Dugdale, R. Tediosi, M. Chergui, and F. Carbone, *Evidence for a Peierls phase-transition in a three-dimensional multiple charge-density waves solid*, Proc. Natl. Acad. Sci. **109**, 5603 (2012).

[20] F. Novelli, D. Fausti, J. Reul, F. Cilento, P. H. Van Loosdrecht, A. A. Nugroho, T. T. Palstra, M. Grüninger, and F. Parmigiani, *Ultrafast optical spectroscopy of the lowest energy excitations in the Mott insulator compound YVO_3: Evidence for Hubbard-type excitons*, Phys. Rev. B **86**, 165135 (2012).

[21] M. Eckstein and P. Werner, *Photoinduced states in a Mott insulator*, Phys. Rev. Lett. **110**, 126401 (2013).

[22] S. Uchida, K. Tamasaku, and S. Tajima, *c-axis optical spectra and charge dynamics in $La_{2-x}Sr_xCuO_4$*, Phys. Rev. B **53**, 14558 (1996).

[23] J. J. Li, J. Chen, D. A. Reis, S. Fahy, and R. Merlin, *Optical probing of ultrafast electronic decay in Bi and Sb with slow phonons*, Phys. Rev. Lett. **110**, 047401 (2013).

[24] S. Nimori, S. Sakita, F. Nakamura, T. Fujita, H. Hata, N. Ogita, and M. Udagawa, *Electron-phonon interaction in $La_{2-x}Sr_xCuO_4$ investigated by Raman scattering*, Phys. Rev. B **62**, 4142 (2000).

[25] B. Mansart, J. Lorenzana, A. Mann, A. Odeh, M. Scarongella, M. Chergui, and F. Carbone, *Coupling of a high-energy excitation to superconducting quasiparticles in a cuprate from coherent charge fluctuation spectroscopy*, Proc. Natl. Acad. Sci. **110**, 4539 (2013).

[26] A. Comanac, L. deMedici, M. Capone, and A. J. Millis, *Optical conductivity and the correlation strength of high-temperature copper-oxide superconductors*, Nat. Phys. **4**, 287 (2008).

[27] L. Hozoi, S. Nishimoto, G. Kalosakas, D. B. Bodea, and S. Burdin, *Nonlocal interactions in doped cuprates: Correlated motion of Zhang-Rice polarons*, Phys. Rev. B **75**, 024517 (2007).

[28] L. Perfetti, P. A. Loukakos, M. Lisowski, U. Bovensiepen, H. Berger, S. Biermann, P. Cornaglia, A. Georges, and M. Wolf, *Time evolution of the electronic structure of 1T-TaS_2 through the insulator-metal transition*, Phys. Rev. Lett. **97**, 067402 (2006).

[29] S. Hellmann, T. Rohwer, M. Kalläne, K. Hanff, C. Sohrt, A. Stange, A. Carr, M. Murnane, H. Kapteyn, L. Kipp, *et al.*, *Time-domain classification of charge-density-wave insulators*, Nat. Commun. **3**, 1069 (2012).

[30] S. De Jong, R. Kukreja, C. Trabant, N. Pontius, C. Chang, T. Kachel, M. Beye, F. Sorgenfrei, C. Back, B. Bräuer, *et al.*, *Speed limit of the insulator–metal transition in magnetite*, Nat. Mat. **12**, 882 (2013).

[31] A. Cavalleri, T. Dekorsy, H. H. Chong, J.-C. Kieffer, and R. W. Schoenlein, *Evidence for a structurally-driven insulator-to-metal transition in VO_2: A view from the ultrafast timescale*, Phys. Rev. B **70**, 161102 (2004).

[32] C. Kübler, H. Ehrke, R. Huber, R. Lopez, A. Halabica, R. F. Haglund Jr, and A. Leitenstorfer, *Coherent structural dynamics and electronic correlations during an ultrafast insulator-to-metal phase transition in VO_2*, Phys. Rev. Lett. **99**, 116401 (2007).

[33] V. R. Morrison, R. P. Chatelain, K. L. Tiwari, A. Hendaoui, A. Bruhács, M. Chaker, and B. J. Siwick, *A photoinduced metal-like phase of monoclinic VO_2 revealed by ultrafast electron diffraction*, Science **346**, 445 (2014).

[34] A. Lanzara, P. V. Bogdanov, X. J. Zhou, S. A. Kellar, D. L. Feng, E. D. Lu, T. Yoshida, H. Eisaki, A. Fujimori, K. Kishio, *et al.*, *Evidence for ubiquitous strong electron–phonon coupling in high-temperature superconductors*, Nature **412**, 510 (2001).

[35] P. D. Johnson, T. Valla, A. V. Fedorov, Z. Yusof, B. O. Wells, Q. Li, A. R. Moodenbaugh, G. D. Gu, N. Koshizuka, C. Kendziora, S. Jian, and D. G. Hinks, *Doping and temperature dependence of the mass enhancement observed in the cuprate* $Bi_2Sr_2CaCu_2O_{8+\delta}$, Phys. Rev. Lett. **87**, 177007 (2001).

[36] F. Ronning, K. M. Shen, N. P. Armitage, A. Damascelli, D. Lu, Z.-X. Shen, L. L. Miller, and C. Kim, *Anomalous high-energy dispersion in angle-resolved photoemission spectra from the insulating cuprate $Ca_2CuO_2Cl_2$*, Phys. Rev. B **71**, 094518 (2005).

[37] J. Graf, G.-H. Gweon, K. McElroy, S. Y. Zhou, C. Jozwiak, E. Rotenberg, A. Bill, T. Sasagawa, H. Eisaki, S. Uchida, *et al.*, *Universal high energy anomaly in the angle-resolved photoemission spectra of High temperature superconductors: Possible evidence of spinon and holon branches*, Phys. Rev. Lett. **98**, 067004 (2007).

[38] N. Gedik, D.-S. Yang, G. Logvenov, I. Bozovic, and A. H. Zewail, *Nonequilibrium Phase Transitions in Cuprates Observed by Ultrafast Electron Crystallography*, Science **316**, 425 (2007).

[39] B. Moritz, F. Schmitt, W. Meevasana, S. Johnston, E. M. Motoyama, M. Greven, D. H. Lu, C. Kim, R. T. Scalettar, Z. X. Shen, and T. P. Devereaux, *Effect of strong correlations on the high energy anomaly in hole-and electron-doped high-T_c superconductors*, New J. Phys. **11**, 093020 (2009).

[40] S. Johnston, F. Vernay, B. Moritz, Z.-X. Shen, N. Nagaosa, J. Zaanen, and T. P. Devereaux, *Systematic study of electron-phonon coupling to oxygen modes across the cuprates*, Phys. Rev. B **82**, 064513 (2010).

[41] J. D. Rameau, S. Freutel, A. F. Kemper, M. A. Sen-

tef, J. K. Freericks, I. Avigo, M. Ligges, L. Rettig, Y. Yoshida, H. Eisaki, J. Schneeloch, R. D. Zhong, Z. J. Xu, G. D. Gu, P. D. Johnson, and U. Bovensiepen, *Energy dissipation from a correlated system driven out of equilibrium*, Nat. Commun. **7**, 13761 EP (2016).

[42] K. M. Shen, F. Ronning, D. H. Lu, W. S. Lee, N. J. C. Ingle, W. Meevasana, F. Baumberger, A. Damascelli, N. P. Armitage, L. L. Miller, Y. Kohsaka, M. Azuma, M. Takano, H. Takagi, and Z.-X. Shen, *Missing quasiparticles and the chemical potential puzzle in the doping evolution of the cuprate superconductors*, Phys. Rev. Lett. **93**, 267002 (2004).

[43] N. Mannella, W. L. Yang, X. J. Zhou, H. Zheng, J. F. Mitchell, J. Zaanen, T. P. Devereaux, N. Nagaosa, Z. Hussain, and Z.-X. Shen, *Nodal quasiparticle in pseudogapped colossal magnetoresistive manganites*, Nature **438**, 474 (2005).

[44] M. Ikeda, M. Takizawa, T. Yoshida, A. Fujimori, K. Segawa, and Y. Ando, *Chemical potential jump between the hole-doped and electron-doped sides of ambipolar high-T_c cuprate superconductors*, Phys. Rev. B **82**, 020503 (2010).

[45] O. Rösch, O. Gunnarsson, X. J. Zhou, T. Yoshida, T. Sasagawa, A. Fujimori, Z. Hussain, Z. X. Shen, and S. Uchida, *Polaronic behavior of undoped high-T_c cuprate superconductors from angle-resolved photoemission spectra*, Phys. Rev. Lett. **95**, 227002 (2005).

[46] R. Mankowsky, M. Först, and A. Cavalleri, *Non-equilibrium control of complex solids by nonlinear phononics*, Rep. Prog. Phys. **79**, 064503 (2016).

[47] A. Subedi, A. Cavalleri, and A. Georges, *Theory of nonlinear phononics for coherent light control of solids*, Phys. Rev. B **89**, 220301 (2014).

[48] S. Maehrlein, A. Paarmann, M. Wolf, and T. Kampfrath, *Terahertz sum-frequency excitation of a Raman-active phonon*, Phys. Rev. Lett. **119**, 127402 (2017).

[49] T. Terashige, T. Ono, T. Miyamoto, T. Morimoto, H. Yamakawa, N. Kida, T. Ito, T. Sasagawa, T. Tohyama, and H. Okamoto, *Doublon-holon pairing mechanism via exchange interaction in two-dimensional cuprate Mott insulators*, Science Adv. **5**, eaav2187 (2019).

[50] P. Giannozzi, O. Andreussi, T. Brumme, O. Bunau, M. B. Nardelli, M. Calandra, R. Car, C. Cavazzoni, D. Ceresoli, M. Cococcioni, *et al.*, *Advanced capabilities for materials modelling with quantum ESPRESSO*, J. Phys. Cond. Matt. **29**, 465901 (2017).

[51] C. L. Reis, J. M. Pacheco, and J. L. Martins, *First-principles norm-conserving pseudopotential with explicit incorporation of semicore states*, Phys. Rev. B **68**, 155111 (2003).

[52] J. P. Perdew and A. Zunger, *Self-interaction correction to density-functional approximations for many-electron systems*, Phys. Rev. B **23**, 5048 (1981).

[53] H. J. Monkhorst and J. D. Pack, *Special points for Brillouin-zone integrations*, Phys. Rev. B **13**, 5188 (1976).

[54] H. Takahashi, H. Shaked, B. A. Hunter, P. G. Radaelli, R. L. Hitterman, D. G. Hinks, and J. D. Jorgensen, *Structural effects of hydrostatic pressure in orthorhombic $La_{2-x}Sr_xCuO_4$*, Phys. Rev. B **50**, 3221 (1994).

[55] The Questaal code is freely available at http://www.questaal.org. Our *GW* implementation was adapted from the original ecalj package, now at https://github.com/tkotani/ecalj/.

[56] D. Pashov, S. Acharya, W. R. L. Lambrecht, J. Jackson, K. D. Belashchenko, A. Chantis, F. Jamet, and M. van Schilfgaarde, *Questaal: a package of electronic structure methods based on the linear muffin-tin orbital technique*, arXiv preprint 1907.06021 (2019).

[57] M. Reehuis, C. Ulrich, K. Prokeš, A. Gozar, G. Blumberg, S. Komiya, Y. Ando, P. Pattison, and B. Keimer, *Crystal structure and high-field magnetism of La_2CuO_4*, Phys. Rev. B **73**, 144513 (2006).

[58] K. Haule, *Quantum Monte Carlo impurity solver for cluster dynamical mean-field theory and electronic structure calculations with adjustable cluster base*, Phys. Rev. B **75**, 155113 (2007).

APPENDIX: METHODS

A. Single crystal growth and characterization

Polycrystalline LCO was prepared by a solid state reaction. The starting materials La_2O_3 and CuO with 99.99% purity were mixed and ground. This process was followed by a heat treatment in air at 900°C-1050°C for at least 70 hours with several intermediate grindings. The phase purity of the resulting compound was checked with a conventional x-ray diffractometer. The resulting powder was hydrostatically pressed into rods (7 mm in diameter) and subsequently sintered at 1150°C for 20 hours. The crystal growth was carried out using an optical floating zone furnace (FZ-T-10000-H-IV-VP-PC, Crystal System Corp., Japan) with four 300 W halogen lamps as heat sources. The growing conditions were as follows: the growth rate was 1 mm/h, the feeding and seeding rods were rotated at about 15 rpm in opposite directions to ensure the liquid's homogeneity, and an oxygen and argon mixture at 3 bar pressure was applied during growth. The as-grown crystals were post-annealed at 850°C in order to release the internal stress and to adjust the oxygen content. One crystal was oriented in a Laue diffractometer, cut along a plane containing the a and c axes and polished to optical quality. Initially, the Néel temperature was determined to be $T_N = 260$ K, which corresponds to a doping $\delta = 3 \times 10^{-3}$ and a hole content $p = 6 \times 10^{-3}$. For this reason, the crystal was annealed for 48 hours to remove part of the excess oxygen. After the treatment, T_N increased to 307 K, which well agrees with the typical value found in purely undoped compounds.

B. Ellipsometry

We used spectroscopic ellipsometry to measure the complex dielectric function of the sample, covering the spectral range from 0.80 eV to 6.00 eV. The experiments were performed using a Woollam VASE ellipsometer. The LCO single crystal was mounted in a helium flow cryostat, allowing measurements from room temperature down to 10 K. The measurements were performed at $<10^{-8}$ mbar to prevent measurable ice condensation onto the sample. Anisotropy corrections were performed using standard numerical procedures.

C. Ultrafast broadband optical spectroscopy.

For the ultrafast optical experiments, we used an amplified laser system operating at a repetition rate of 3 kHz. The set-up is based on a Ti:Sapphire oscillator, pumped by a continuous-wave Nd:YVO_4 laser, emits sub-50 fs pulses at 1.55 eV with a repetition rate of 80 MHz. The output of the oscillator seeds a cryo-cooled Ti:Sapphire amplifier, which is pumped by a Q-switched Nd:YAG laser. This laser system provides ∼45 fs pulses at 1.55 eV. One third of the output, representing the probe beam, is sent to a motorized delay line to set a controlled delay between pump and probe. The 1.55 eV beam is focused on a 3 mm-thick CaF_2 cell using a combination of a lens with short focal distance and an iris to limit the numerical aperture of the incoming beam. The generated continuum covers the 1.77-2.90 eV spectral range. The probe is subsequently collimated and focused onto the sample through a pair of parabolic mirrors at a small angle from normal incidence. The remaining two thirds of the amplifier output, representing the pump beam, are frequency doubled to 3.10 eV in a β-barium borate crystal and directed towards the sample under normal incidence. Along the pump path, a chopper with a 60 slot plate is inserted, operating at 1.5 kHz and phase-locked to the laser system. Both pump and probe are focused onto the sample on spots of dimensions 120 μm × 87 μm for the pump and 23 μm × 23 μm for the probe. The sample is mounted inside a closed-cycle cryostat, which provides a temperature-controlled environment in the range 10-340 K. The reflected probe is dispersed by a fiber-coupled 0.3 m spectrograph and detected on a shot-to-shot basis with a complementary metal-oxide-semiconductor linear array. Before the data analysis, the transient reflectivity matrix was corrected for the group velocity dispersion of the probe. It is important to note that the probe beam dispersion is not a limiting factor for the time resolution of the setup, since it is given on the detection side by the much smaller effective pulse duration per detector pixel. As such, the time resolution of the setup for all probe photon energies is ∼50 fs.

D. Ab initio calculations.

Phonon calculations. To characterize the lattice modes of LCO, we performed density-functional theory linear-response calculations as implemented in the Quantum Espresso package [50]. We used norm-conserving pseudopotentials explicitly including semi-core states [51] for La and Cu, the local density approximation (LDA) [52], and a plane-wave cutoff energy of 200 Ry on the kinetic energy. The charge density and dynamical matrices were calculated for the Γ point of the Brillouin zone using a 7 × 7 × 7 Γ-centered Monkhorst-Pack [53] electron-momentum grid and a Gaussian smearing of 0.002 Ry. The convergence with respect to all these parameters has been checked thoroughly. The experimental primitive unit cell [54] was relaxed prior to the phonon calculation which resulted in a slightly reduced volume (∼1%), typical for LDA calculations.

QSGW+DMFT calculations. We modelled the optical data of LCO by combining the QSGW theory and DMFT calculations [5], as implemented in the Questaal package [55, 56]. The paramagnetic DMFT is com-

bined with the QSGW via local Cu-3d projectors of the Kohn-Sham space to the correlated subspace. We carried out the calculations for non-magnetic LCO in the orthorhombic phase with space-group 64/Cmca [57], within the QSGW+DMFT approach. DMFT provides a non-perturbative treatment of the local spin fluctuations. We use hybridization expansion flavor of locally exact continuous time quantum Monte-Carlo solver (CT-QMC) [58] to solve the correlated impurity problem. Charge self-consistency on the static QSGW potential is performed on a $16 \times 16 \times 16$ k-mesh, fully converging the charge. The GW self-energy (Σ^0), which varies with k much more slowly than the kinetic energy, is calculated on a $4 \times 4 \times 4$ k-mesh, and converged with RMS change in $\Sigma^0 < 10^{-5}$ Ry. Subsequent DMFT calculations are iterated, and the dynamical self-energy converges in $\sim$15-20 iterations. The calculations for the single particle responses are performed with 10^8 QMC steps per core and the statistics is averaged over 64 cores. As a second step, we considered a small rigid displacement of the ionic positions in LCO along the phonon vector fields calculated from density-functional theory. Finally, we computed the in-plane optical conductivity for the different displaced structures. The largest amplitude of the considered shifts were 0.04 Å.